Received: 31 July 2011 ■ *Revised: 30 November 2011* ■ *Accepted: 7 December 2011* ■ *Publication: 6 March 2012*

JNIRS JOURNAL OF NEAR INFRARED SPECTROSCOPY

Special Issue on Medical Applications

Review

Near infrared spectroscopy in optical coherence tomography

Chenyu Wang, Jinman Kim, Craig T. Jin, Philip H.W. Leong and Alistair McEwan*

School of Electrical and Information Engineering, The University of Sydney, NSW, Australia, 2006. E-mail: alistair.mcewan@sydney.edu.au

Optical coherence tomography (OCT) is a technique that is able to provide cross section views of tissue layers. This fast and non-invasive method is widely used in clinical applications for the diagnosis and treatment of certain diseases. Although conventional OCT is derived from the theory of interferometric imaging, emerging developments, including spectroscopic OCT and related techniques such as dual-band OCT and Raman spectroscopy–OCT, have resulted in significantly improved clinical capabilities for observing the tissue layers through enhanced tissue definition, image resolution, image contrast and scanning speed. This paper reviews the state-of-the-art developments of OCT. It starts with a general introduction of conventional interferometric OCT imaging methods including the time-domain and frequency-domain techniques. The second section explores the advances introduced from spectroscopy techniques in OCT, especially with spectroscopic OCT, dual-band OCT and Raman spectroscopy combined OCT. The final section discusses the current challenges in the application of approaches based on computer-aided diagnosis (CAD) for retinal imaging, for example automated segmentation of tissue layers and tracking disease progression. This task is currently limited by the quality of the recorded data from OCT systems but will be improved by adopting spectroscopic techniques. Finally, we analyse and discuss the improvements that are expected in retinal CAD from the adoption of newly emerging near infrared spectroscopy OCT at multiple wavelengths.

Keywords: near infrared spectroscopy, optical coherence tomography spectroscopy, ophthalmology, retinal imaging

Introduction

Optical coherence tomography (OCT) is a novel imaging technique that is able to rapidly and non-invasively produce high-resolution images of biological tissue at a micrometre scale. This technique was first demonstrated in the imaging of retinal cross-layer structures by Fujimoto *et al.* in 1991.[1] OCT instrumentation has since become a powerful clinical tool for the diagnosis of disease and investigation of pathology in many clinical fields,[2–5] particularly ophthalmology.[6–10] Using OCT, the sub-surface of retinal layers behind the nerve fibre layer can easily be observed (Figure 1). This feat was not possible with previous techniques, such as fluorescein angiography or retinal ultrasound. It not only provides an excellent diagnostic method for the investigation of the structure and thickness of retinal layers, but also enables the tracking of changes following treatment and assists with the planning of treatment, which is important for new therapy and drug development. Besides ophthalmology, OCT is playing an essential role in cardiology, oncology, dentistry, surgery, neurology, reproductive medicine and other areas.[3,5]

OCT is an interferometric technique that measures the interference between a reflected reference wave and a back-scattered wave from the tissue sample. The interference signal provides information regarding the depth and location of tissue structures. In general, it takes advantage of the

ISSN: 0967-0335
doi: 10.1255/jnirs.975

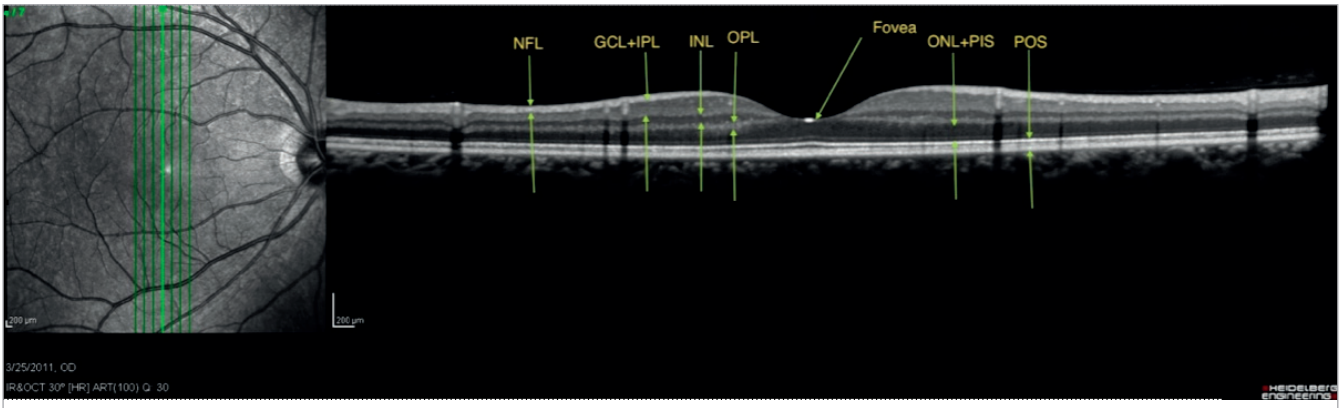

Figure 1. OCT image near the fovea of the lead author's retina, acquired in The Save Sight Institution, University of Sydney. Instrument: Spectralis HRA+OCT, Heidelberg Engineering, Heidelberg Germany. Left is the retina surface image, and right is the OCT image scanned along the vertical bright green line as showed in the left picture. NFL, nerve fibre layer; GCL, ganglion cell layer; IPL, inner plexiform layer; INL, inner nuclear layer; OPL, outer plexiform layer; ONL, outer nuclear layer, PIS, Photoreceptor inner segments; POS, photoreceptor outer segments. (All colour figures can be seen in colour on the web).

coherence properties of light to detect properties of the tissue or material at a micrometre scale.

There are several types of OCT which have been developed with varying features. OCT technologies can be classified as time domain OCT (TD-OCT), frequency domain OCT (FD-OCT), spectroscopic OCT (SOCT) and dual-band OCT. TD-OCT uses the traditional Michelson interferometer technique. FD-OCT removes the need for a moving mirror by using Fourier techniques on electronically recorded two-dimensional interference patterns at multiple optical delay times. SOCT uses localised spectral analysis methods such as the short-time Fourier transform (STFT) or the wavelet transform to recover spectroscopic information at different depths. STFT suffers from a trade-off between time and frequency resolution. This is somewhat alleviated with DB-OCT where a double peak spectrum is applied to the sample and the coherence is detected with an individual spectrometer for each wavelength band.

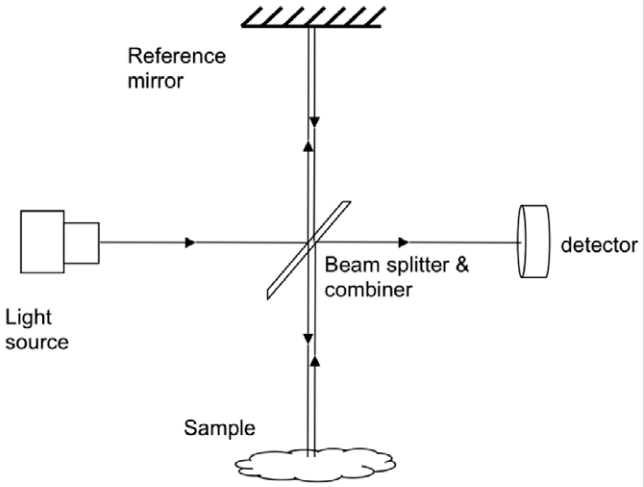

Figure 2. Schematic of Michelson interferometer.

Time-domain optical coherence tomography

TD-OCT is based on the Michelson interferometer (Figure 2), where a broadband continuous light source is split via a 50/50 beam splitter. One light beam travels along the sample arm towards the subject and the other propagates towards a flexible (moving) reference mirror. The reflected light beams from both reference mirror and sample arm are combined by the coupler and a part of this signal is transferred to the detector. The interference bands can be measured by the detector if the optical path length difference of the two beams is less than the coherence length. The coherence length varies inversely with the bandwidth of the light source.[4] Since the position of reference mirror for a specific visible band is related to the distance from the light-reflecting surface, the interference signal provides a reflectivity profile or depth information. This depth information is referred to as the "A-scan". A cross section of depth information, "B-scan", can be built up through scanning the sample laterally, either by moving the sample under test or moving the light on the sample. Combining the A- and B-scans results in the full three-dimensional scan as illustrated in Figure 3. Alternatively, a "C-scan" or "en-face" slice can be obtained at a specific depth, as illustrated in Figure 4.

TD-OCT has been applied in many medical applications, but its relatively slow scan speed limits its performance for investigating large volumes of tissue, particularly since speed is closely related to the scan detection sensitivity.[11] The development of FD-OCT has overcome this weakness.

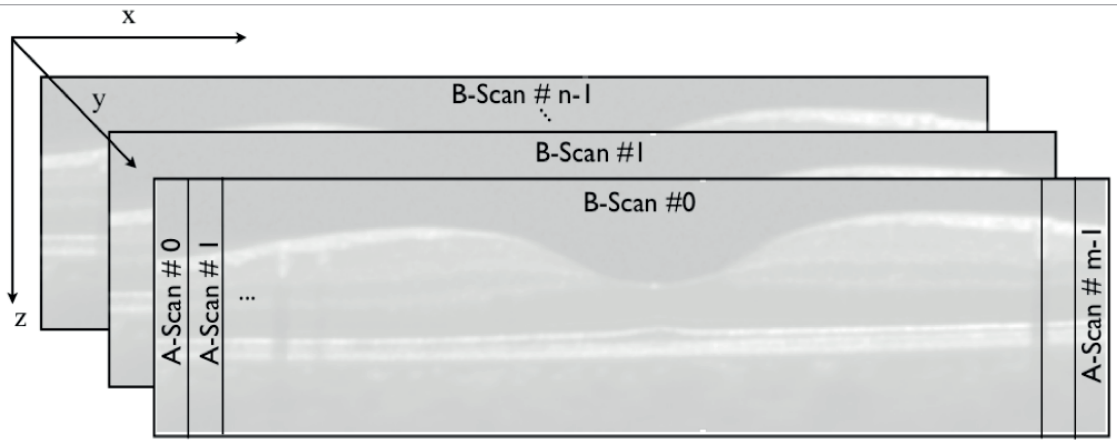

Figure 3. OCT scan dimensions: A-scan and B-scan.

Frequency domain optical coherence tomography

The first medical application of FD-OCT was demonstrated in 1995 by Fercher *et al.*[12] Since then, the development of FD-OCT has concentrated on increasing acquisition speed[11,13] and this has transformed OCT technology to a comprehensive micrometre scale imaging technology, enabling many new clinical applications.[14] FD-OCT uses a similar broadband light source and spectrometer to TD-OCT, but differs in that (1) the mirror in the reference channel remains stationary and (2) the interference signal is acquired in a spectrally separated fashion (see Figure 5 and Figure 6). By applying the Fourier transform, the required depth image can be obtained. The spectral separation is performed using a spectrally scanning source to encode the optical frequency in time, or with spectrally separated detector such as a fibre Bragg grating or a linear detector array based on photodiode arrays, charge coupled device (CCD) or image sensors.[15]

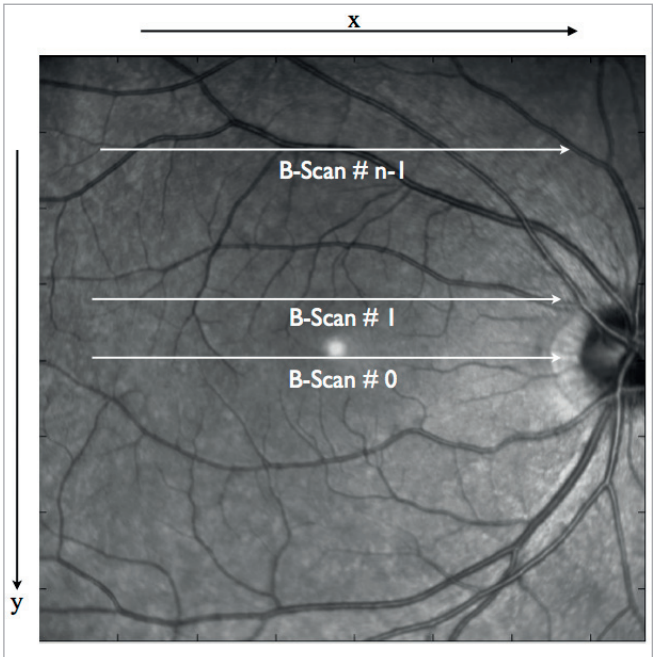

Figure 4. OCT scan dimensions: en-face (retina).

FD-OCT has higher detecting sensitivity than TD-OCT, even in low light conditions[16] and can operate at a faster speed as mechanical movement of mirrors is not necessary. As a result, high-resolution imaging with reduced motion artefacts, one of the major issues in TD-OCT,[3] is possible. Motion artefacts still exist in spectral domain and optical frequency domain imaging, for example in retinal imaging where involuntary eye movements or micro saccades occur.[17] As the Fourier transform process used in FD-OCT involves the integration of the entire dataset obtained in a single A-line measurement,[17] any movement during a single A-scan will corrupt the resulting image. Current state-of-art techniques using FD-OCT allow cross-section image acquisition speeds of greater than 100,000 A-scans per second. Such high-speed OCT instrumentation is increasingly demanded in contemporary medical applications.[18]

During the last decade, many issues in TD-OCT and FD-OCT have been solved by integrating spectroscopy technology. This is a rapidly growing and intense area of development. In the next section, a review of new spectroscopy techniques that have improved the state of the art OCT is presented.

Spectroscopic optical coherence tomography

Spectroscopy has been widely used for investigating the structure and chemical composition of materials. SOCT[19] integrates the interference measurement with a measurement of the spectroscopic properties in a single scan. This complementary spectral information may be used to improve the OCT image contrast and to overlay false colour spectroscopic information

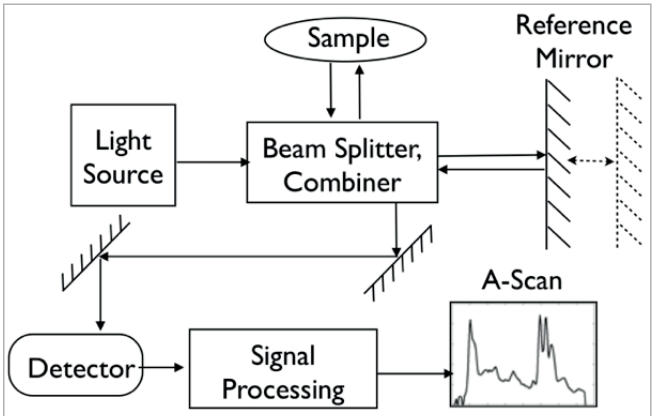

Figure 5. Schematic of TD-OCT.

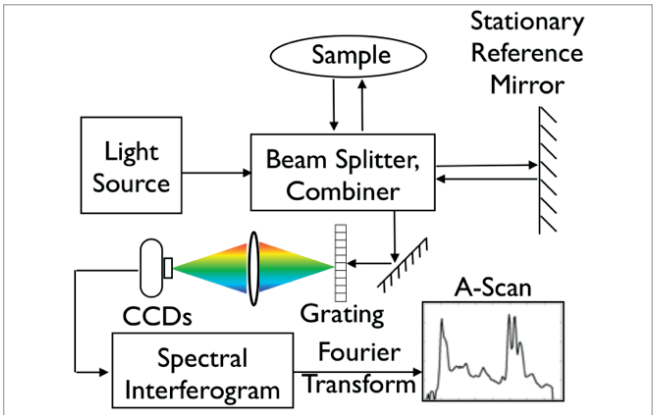

Figure 6. Schematic of FD-OCT.

on the grey-scale OCT depth scan. The process can be viewed as a spectroscopic staining in an analogous way to histological staining.[20]

In SOCT, alternative digital signal processing is performed on both the intensities and the spectra of the back-scattered light. One difficulty with this approach is that the spectrum varies with depth along the imaging axis, leading to SOCT signals that are not stationary with respect to depth or frequency. These signals can not be analysed directly with the Fourier transform and, hence, SOCT uses localised spectral analysis methods such as the STFT or wavelet transform to recover spectroscopic information at different depths.[21]

SOCT provides additional spectral information with the broadband light source of either TD-OCT or FD-OCT (Figure 7). In TD-OCT, the SOCT signal is obtained by applying the STFT on the time interferogram over a time delay window with size $\Delta\tau$. The SOCT signal obtained is the spectrum in the window region at each depth. Similarly, a method called the short frequency Fourier transform (SFFT),[22] in which the dual of the STFT in the frequency domain is applied on the spectral interferogram in FD-OCT. The calculated SOCT signal contains the depth dependent spectral information in the bandwidth ω to $\omega+\Delta\omega$.

The performance of this localised spectral analysis is limited by an inherent trade-off between time and frequency based on the uncertainty principle. An increase in spectral resolution leads to a decrease in time resolution ultimately leading to a decrease in depth information or image resolution in the SOCT image. For instance, in Figure 7, the increase of window size, $\Delta\tau$, for time domain SOCT includes greater spectrum information; however, the total number of STFT sub-samples is decreased, leading to lower SOCT image resolution. Usually, in SOCT "time" refers to depth and "frequency" refers to wavelength so this trade-off is also referred to as the "depth–wavelength" trade-off.

By reviewing the major signal processing techniques for SOCT, Oldenburg *et al.*[23] indicated that there is no single SOCT instrument that can be optimised for all biological tissue applications. This is due to the many varieties of parameters

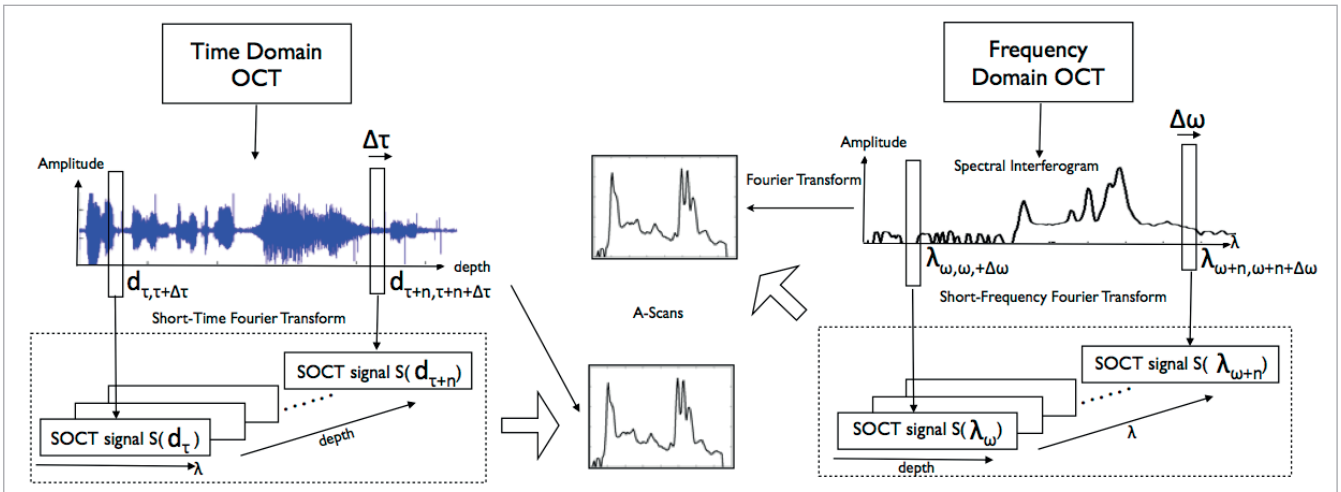

Figure 7. Spectroscopic OCT with time-domain OCT (left) and frequency domain OCT (right). STFT and SFFT are performed on TD-OCT and FD-OCT, respectively.[23]

that need to be defined for a chosen scenario, including those of the instruments and trade-offs between hardware and software. As an example, "Imaging lens numerical aperture, operating bandwidth, time–frequency transformation, computation of the appropriate metrics, incoherent signal averaging and multi-channel image display",[23] all need to be considered. Due to the complex structure of living tissue and their variable scattering properties, it is also very difficult to have a stationary attenuation coefficient for different tissue structures. Hermann *et al.*[24] demonstrated a method called dispersion encoded full range algorithm (DEFR) for full range analysis of spectroscopic OCT, where they discussed the demand for proper calibration to minimise chromatic aberrations. Following this research, Steiner *et al.*[25] further analysed the influence on the spectral absorption measurement from autocorrelation terms in SOCT, through a simplified OCT system design.

Studies of SOCT have found that the spectra of backscattered light changes with its depth and wavelength. Hence, SOCT must face the trade-off between frequency resolution and time resolution. Not surprisingly, there is no best time–frequency distribution (TFD)[21] that can solve all the problems and different types of TFDs along with different parameters need to be chosen for optimising time–frequency trade-offs in variable scenarios. In 2005, Xu *et al.*[26] discussed the applications of SOCT based on wavelength-dependent scattering. By combining light scattering spectroscopy and SOCT, this could provide a more sensitive and localised indicator than spectral absorption.

Although SOCT has efficiently enhanced the contrast of OCT images, the problem of low contrast still remains because some human tissues are not spectrally active in the associated operation band. Hence, the investigation of contrast agents for SOCT is increasingly important. In 2004, Xu *et al.*[27] demonstrated a method for enhancing image contrast by applying near infrared (NIR) dyes as contrast agents with those absorption spectra characteristics in SOCT. One associated problem is that NIR dyes absorb optical power, reducing the image measurement depth approximately 20–30%. Recently, Cang *et al.*[28] have investigated the potential of using gold nanocages as contrast agents for SOCT. Experimental results showed that these have a large absorption cross section and an easy tuneable optical resonance peak. This has the potential to be one of the optimal contrast agents for OCT imaging.

Medical applications of spectroscopic optical coherence tomography

Most applications of spectroscopic OCT are non-invasive measurements of blood glucose levels and blood oxygen saturation and for the detection of precancerous cells.[29] Here we consider blood oxygen saturation (SaO_2) measurements as one example.

Tissue oxygenation is an important biological indicator for many diseases, such as cancer, inflammatory disease, diabetic retinopathy, choroidal disorders, stroke etc.[30] In the last decade, the development of spectroscopy OCT has improved the efficiency of measuring the saturation of blood oxygen. In 2003, Faber *et al.*[31] demonstrated the measurements of haemoglobin and oxygenated haemoglobin by using spectroscopic OCT. At that time, the major limit was slow imaging due to the dynamic focusing of the OCT system. Two years later, a quantitative correlation between the measured differential attenuation coefficient and saturation was found by the same group.[32] The concept of spectroscopic spectral OCT was used by Lu *et al.*[33] and his group to develop an alternative approach that simplified the operation procedures for examining haemoglobin oxygen saturation level, avoiding the need for calibration of the absolute absorption coefficient of each subject.

Recently, there have been several improvements on the measurement of SaO_2 by using spectroscopic OCT. Yi and Li[34] discovered that there is a reliable linear relationship between the oxygen saturation measured from spectroscopic OCT and diffusive spectroscopy measurement. This indicated the great potential for SaO_2 assessment using SOCT from individual erythrocytes. The quantitative measurement of SaO_2 has been improved by reducing the speckle noise in the image, as well as eliminating the spectral modulation.[35] These developments of SOCT have led to more complex measurements, for instance, a haemoglobin concentration measurement[36] diagnostic. Since the haemoglobin concentration and oxygen saturation levels are the two essential measurements for various disease diagnoses, including cancer, this could be an important complement to existing diagnostic approaches.

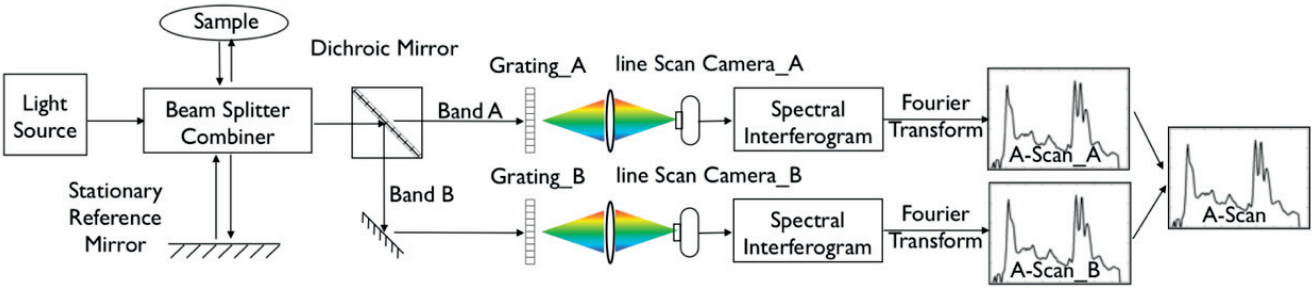

Figure 8. Schematic of dual-band OCT.

Table 1. Recent research in dual-band OCT at different wavelengths.

Researchers	Bands of wavelength	Type of OCT	Description
Spöler *et al.*[38]	840 nm, 1230 nm	Ultra-high resolution OCT	Compared to spectroscopic OCT at single band, data acquisition time and processing time of dual-band OCT is reduced. Contrast is enhanced without contrast agents.
Sacchet *et al.*[39]	800 nm, 1200 nm	Full field OCT[40,41]	Dramatically deceased the acquisition time compared to spectroscopic OCT Provides much more information on spectral than single band OCT. The penetration depth at 1200 nm is better than 800 nm
Cimalla *et al.*[37]	800 nm, 1250 nm	Spectral domain OCT, with a commercial SC laser source	Contrast enhanced
Kray *et al.*[42]	740 nm, 1300 nm	Spectral domain OCT, fibre based	Contrast enhanced. Signal processing is reduced

SC: superconinuum

Dual band optical coherence tomography

Dual-band OCT essentially applies OCT with dual systems at two wavelength bands simultaneously (Figure 8). A source signal with two wavelength bands or a "double peak spectrum" is generated by an optical shaping and spatial filtering. This can be achieved with various combinations of optical and spatial aperture filters in a prism–lens sequence. The beam with the shape of a double peak is applied to the interferometer set-up. The combined interference signal is split into the two wavelength bands by a diachronic mirror and each spectral band is then sent to an individual spectrometer.[37] The benefits of this technique include the enhancement of penetration depth, enhancement of contrast and speckle noise removal by using the uncorrelated information in the two frequency bands. Compared to SOCT over a wide range of spectral components, dual-band OCT has advantages in faster acquisition time and optimisation of the spectrum of interest. Recent advances in the development of dual-band OCT for the near infrared range are listed in Table 1.

Raman spectroscopy combined optical coherence tomography

Another popular combination of NIR modalities is OCT and the weak frequency shift detected in Raman spectroscopy,[43] which measures the small number of scattered photons from a sample illuminated with monochromatic light. These photons exhibit a frequency shift that is related to the vibrational or rotational states of the molecular bonds in the material. Raman spectroscopy is a contrast- and label-free molecular imaging technique. Based on the use of NIR Raman spectroscopy (NIR-RS) in characterisation of living tissues, the combination of NIR-RS and OCT can provide complementary benefits: NIR-RS can provide biochemical specifications of tissues while OCT could indicate the structural characteristic

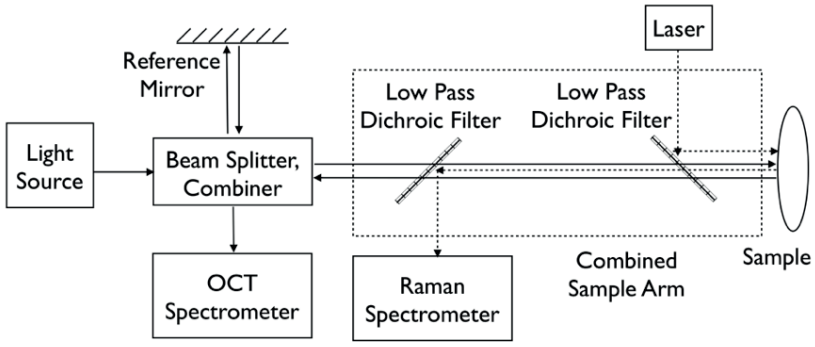

Figure 9. Schematic of combined OCT and Raman spectrometer.

of cells and tissues. In general, OCT could be used to scan large areas of tissue for morphological changes quickly and with a relatively large aperture while the NIR-RS could be used to confirm biochemical or molecular features in a small area of interest. In tissue, the use of Raman spectroscopy is particularly challenging as the source strength must be kept low enough so as not to damage the tissue. Figure 9 shows an example schematic of the Raman-OCT set-up using the common sample arm approach. Patil *et al.*[44] reported an integrated system using a common detector for both Raman shift spectra and OCT signals. They employed a deep depleted, back-illuminated and thermo-electrically cooled CCD array that was sensitive to the weak Raman signal but limited OCT imaging speed to 2 frames s^{-1}.

Patil *et al.* also demonstrated a combined NIR-RS-OCT device applied to skin cancers[45] and showed the potential of this instrument for providing comprehensive morphological and biochemical information from a single tissue scan. OCT scans alone did not clearly depict features of malignancy with normal and basal cell carcinoma (BCC) scans with both showing significant sub-surface reflective features. While the features in the BCC scan were deeper and below the epidermal–dermal boundary, in agreement with previous OCT work on BCC, these sub-dermal features were also seen in OCT scans of scar tissue following removal of a lesion. The Raman spectroscopy shift spectra exhibited clear differences in BCC tissue in the regions centred at 1090 cm^{-1}, 1300 cm^{-1} and 1440 cm^{-1} indicating an increase in spectral contributions of proteins and nucleic acids. These are associated with an increase in the size of the nucleus relative to the cytoplasm and found in tumours. The scar tissue exhibited differences at only one region centred at 1300 cm^{-1} .

In summary, the NIR-RS was found to identify tumours where OCT had morphological changes of interest. Ko *et al.*[46] showed that RS-OCT can provide depth information via OCT on dental carries with Raman spectroscopy by providing the biochemical information on mineral orientation and composition to enable early identification of incipit carriers that are limited only to the outer surface of the tooth. They found that the Raman peaks were sensitive to the geometry of the Raman sampling arrangement suggesting that the enamel is optically anisotropic. In addition, the spectral differences between sound and carious enamel changed with the Raman sampling depth. Hence a Raman probe alone would not be practical for finding lesions unless combined with OCT for identifying suspicious lesions sites and depths for Raman sampling.

Evens *et al.*[47] presented results from a RS-OCT system applied to *ex vivo* retinal tissue. Their set-up was similar to the system used by Patil *et al.*,[44,48] with two key differences: (1) a significantly lower source signal of 4 mW is delivered to the retinal tissue to ensure that it corresponds more closely with the conditions of *in-vivo* imaging and (2) simultaneous illumination of the sample and measurement with both OCT and Raman spectroscopy. The reduction in source signal and short integration time of Raman spectroscopy for simultaneous measurements (200 ms) led to a reduction in Raman spectroscopy signal-to-noise ratio. This was addressed by averaging Raman spectroscopy samples over wide regions of corresponding OCT A-scan samples. While this technique was able to produce results for simple polystyrene phantoms and identify different spectra for the fovea, it was not successful in separating detailed retinal structure in a sample that was possibly compromised by preservatives used in the *ex vivo* sample.

Overall, the combination of OCT and a variety of near infrared spectroscopic technologies has been successful in providing complementary molecular information and in improving the imaging quality from conventional OCT, especially in developing the contrast enhancement, speckle noise reduction and depth increasing penetration. The application described below is an example of such a synergy.

Application of computer-aided diagnosis on retina imaging

After the OCT instrument has acquired the signal and the crosssection images are formed, a computer-aided diagnosis (CAD) system is often used to automate and to assist in image analysis.[49] Due to the multi-dimensional nature of the retina imaging (three-dimensional spatial + temporal), the use of visualisation and digital image processing methods available in CAD such as multi-planar reformatting, automated tissue separation (segmentation) and measurement tools, are becoming ever more essential. CAD has been widely used in retina imaging as a powerful tool for manipulating acquired raw data and it is also an important tool for compensating limitations from the OCT

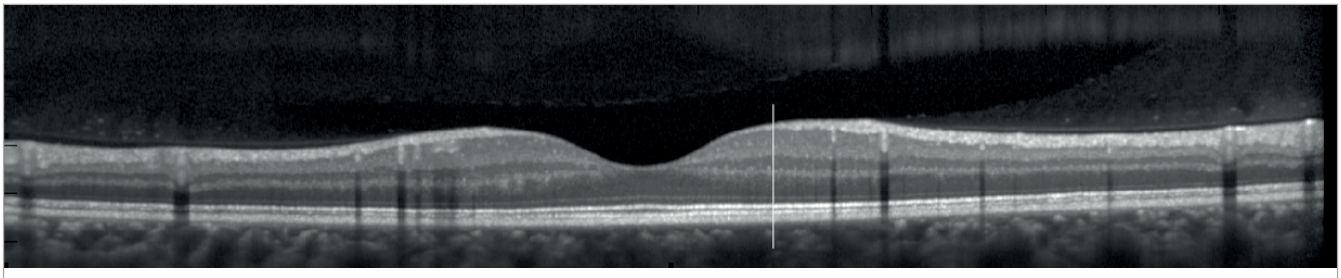

Figure 10. A raw retinal OCT image. The pixel intensities along the bright vertical line are plotted in Figure 12.

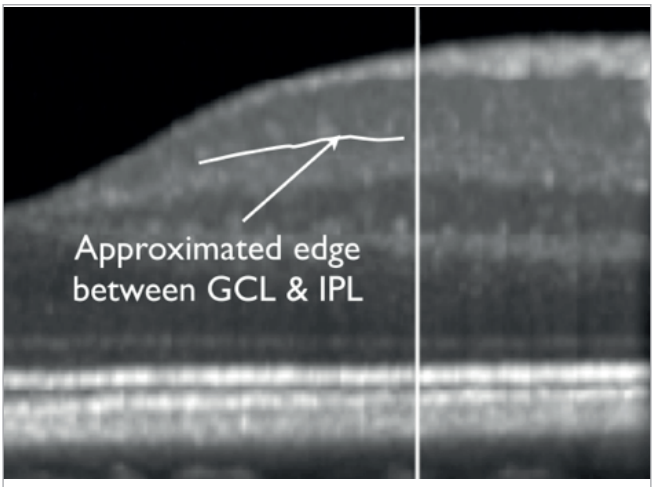

Figure 11. Approximated edge between GCL and IPL layers using computer-aided diagnosis.

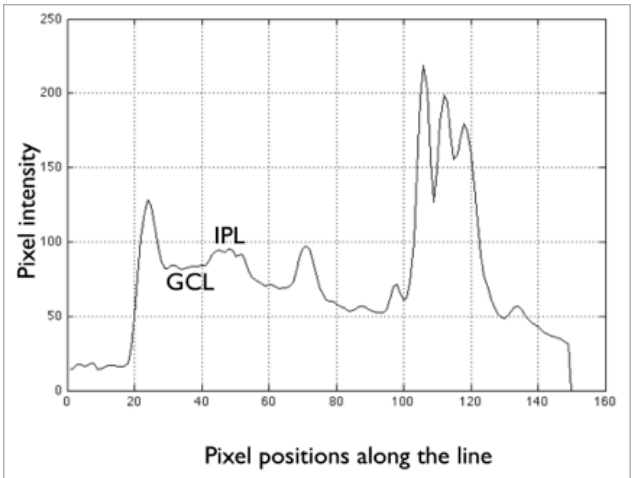

Figure 12. Pixel intensities along the bright vertical line in Figure 10.

hardware. For example, the OCT image has inherent speckle noise which, when combined with low contrast definition,[50] restricts the ability to accurately separate the different tissue layers. In order to improve the image quality, various filters are applied to the OCT images, for example mean filter, median filter, hybrid filter and many others.[50] Moreover, innovative filters have been shown to enhance OCT image contrast and edges.[51] These filters rely on the simple statistics derived from a pixel (or voxel in three-dimensional OCT) and its neighbouring pixels in an attempt to remove speckle noise. As such, the performances of such filters are dependent on manipulating pixel values, particularly the differences between the neighbouring pixels and thus are incapable of distinguishing pixels that are corrupted by high noise.

A raw retinal OCT image is presented as Figure 10. Figure 11 shows the part of the image near the bright vertical line in Figure 10, obtained using a spectral domain OCT (Spectralis HRA+OCT; Heidelberg Engineering, Heidelberg, Germany). The thickness measurement of this area is critical for analysing vision loss from diseases such as optical neuritis or glaucoma.[52,53] Previous research[54–57] has applied automated segmentation to separate most of the retinal tissue layers but they were generally not able to segment the ganglion cells layer (GCL) and the inner plexiform layer (IPL), as these tissues both have very similar optical (pixel intensity) characteristics.

As shown in Figure 11, the border between the GCL and IPL is difficult to distinguish by the naked eye. Figure 12 shows the pixel intensities along the bright vertical line in Figure 10 and it clearly indicates that the gradient of GCL and IPL edge is small, which may lead to unreliable edge detection. In Figure 13, pixel intensity plots of repeated OCT scans at the same location, as shown in Figure 10, show the intensity result of repeating scans following the image of Figure 10 and the intensity profile is sampled at the same position and displayed as the vertical line. Most edges can

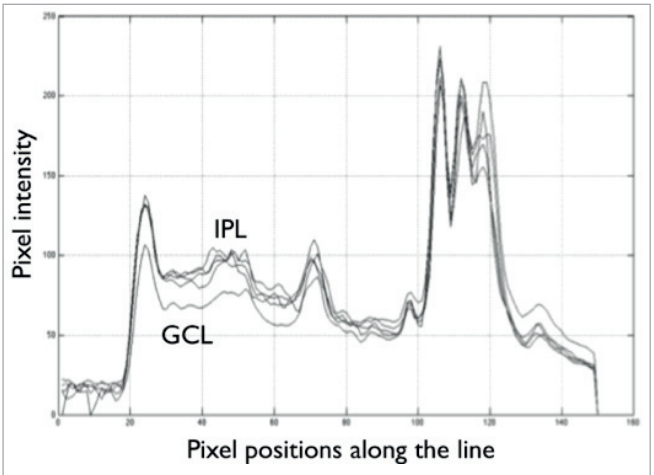

Figure 13. Pixel intensity plots of repeated OCT scans at the same location as shown in Figure 10.

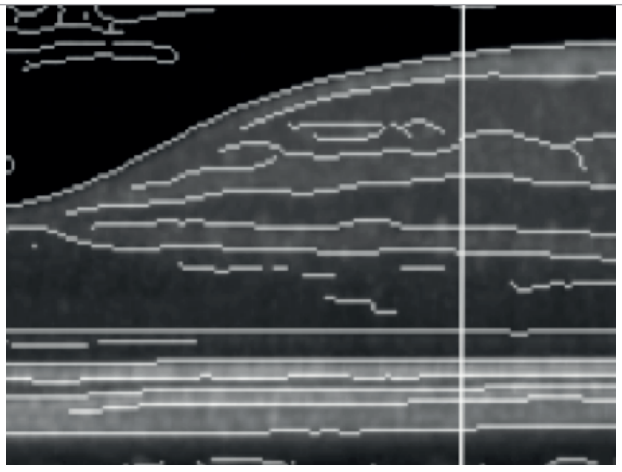

Figure 14. Edge detection result by applying a "Canny" edge detector.[59]

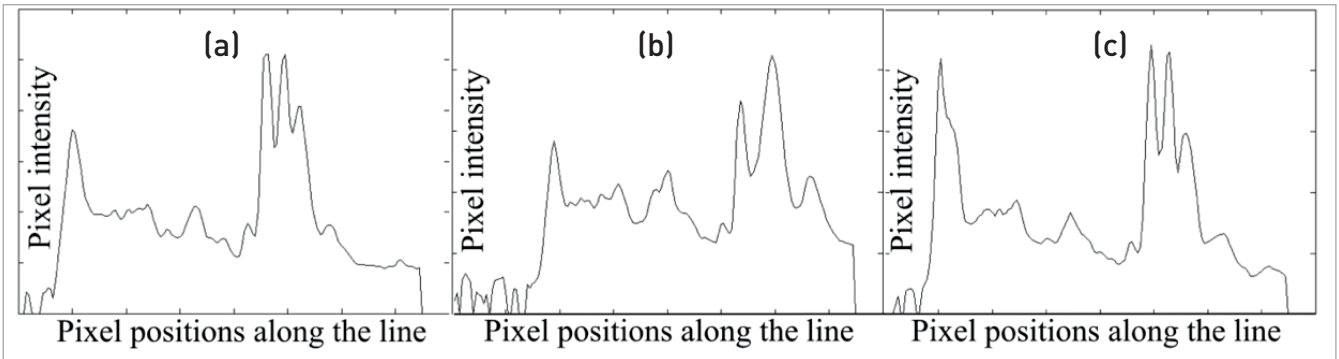

Figure 15. Vertical pixels intensity profile of three different subjects across all retina layers near the fovea.

be identified due to their large gradient except the edge between GCL and IPL, although there is fluctuation between different scans. This phenomenon will cause the unreliable edge detection on the GCL and IPL border. Figure 14 shows the result of the "Canny" edge detection algorithm[58] after median filtering. The small gradient between GCL and IPL could easily cause discontinuities on the detected edges and bring complexity to the further computation, such as edge identification and thickness measurement after edge detection. In fact, the GCL and IPL edge is completely undetectable on most OCT images due to their similar density. Figure 15 shows three examples where the GCL/IPL edges have almost the same intensity.

Thus, it is necessary to look for other solutions to enhance the contrast between the different tissues of the retina. Near infrared SOCT at several wavelengths has been shown to acquire more information regarding tissue types at different penetration depths and improved OCT images within the depth–wavelength trade-off. Dual-band OCT offers this advantage without the trade-off and less speckle noise by exploiting the uncorrelated information in each frequency band. Less speckle noise will relax the requirements on the image processing algorithms for filtering and edge detection. RS-OCT may also offer these benefits but recent work suggests that there are either limitations in Raman spectroscopy signal-to-noise ratio or OCT imaging rates when used in retinal tissues due to concerns in keeping the source signal within the safe range for *in vivo* tissue. Therefore SOCT or dual-band OCT are good contenders for solving this issue in the ophthalmology example above.

Conclusion

The integration of spectroscopy technologies with OCT, such as spectroscopic OCT, dual-band OCT and Raman spectroscopy combined OCT have enhanced the quality of OCT images and provided complementary molecular information. Specifically, the capability of contrast enhancement, speckle noise reduction and penetration depth optimisation on a variety of living tissues has significantly improved the functionality of OCT technology. As described in the ophthalmological example given in this paper, there is a need for improved near infrared spectroscopy OCT for computer-aided diagnosis. By enhancing contrast and reducing speckle noise, the measurements made on retinal layers could be much more accurate and rely less on advanced image processing algorithms.

References

1. D. Huang, E.A. Swanson, C.P. Lin, J.S. Schuman, W.G. Stinson, W. Chang, M.R. Hee, T. Flotte, K. Gregory, C.A. Puliafito and J.G. Fujimoto, "Optical coherence tomography", *Science* **254(5035),** 1178 (1991). doi: 10.1126/science.1957169
2. J.M. Shmitt, "Optical coherence tomography: A review", *IEEE J. Sel. Top. Quantum Electron.* **5(4),** 1205 (1999). doi: 10.1109/2944.796348
3. A.M. Zysk, F.T. Nguyen, A.L. Oldenburg and D.L. Marks, "Optical coherence tomography: A review of clinical development from bench to bedside", *J. Biomed. Opt.* **12(5),** 015403 (2007). doi: 10.1117/1.2793736
4. B.E. Bouma and G.J. Tearney, *Handbook of Optical Coherence Tomography.* Marcel Dekker Inc., New York, USA (2001).
5. M. Brezinski, *Optical Coherence Tomography: Principles and Applications.* Academic Press, Boston, USA (2006).
6. R.A. Costa, M. Skaf, L.A.S. Melo, Jr, D. Calucci, J.A. Cardillo, J.C. Castro, D. Huang and M. Wojtkowski, "Retinal assessment using optical coherence tomography", *Retinal Eye Res.* **25(3),** 325 (2006). doi: 10.1016/j.preteyeres.2006.03.001
7. M.E.J.V. Velthoven, D.J. Faber, F.D. Verbraak, T.G. v. Leeuwen and M.D. d. Smet, "Recent developments in optical coherence tomography for imaging the retina", *Retinal Eye Res.* **26,** 57 (2007). doi: 10.1016/j.preteyeres.2006.10.002
8. W. Drexler and J.G. Fujimoto, "State-of-the-art retinal optical coherence tomography", *Retinal Eye Res.* **27,** 45 (2008). doi: 10.1016/j.preteyeres.2007.07.005
9. S. Wolf and U. Wolf-Schnurrbusch, "Spectral-domain optical coherence tomography use in macular diseases:

A review", *Ophthalmologica* **224,** 333 (2010). doi: 10.1159/000313814

10. M.L. Gabriele, G. Wollstein, H. Ishikawa, L. Kagemann, J. Xu, L.S. Folio and J.S. Schuman, "Optical coherence tomography: History, current status and laboratory work", *Invest. Ophthalmol. Vis. Sci.* **52(5),** 2425 (2011). doi: 10.1167/iovs.10-6312

11. S. Yun, G. Tearney, J.D. Boer, N. Iftimia and B. Bouma, "High-speed optical frequency-domain imaging", *Opt. Express* **11(22),** 2953 (2003). doi: 10.1364/OE.11.002953

12. A.F. Fercher, C.K. Hitzenberger, G. Kamp and S.Y. El-Zaiat, "Measurement of intraocular distances by backscattering spectral interferometry", *Opt. Commun.* **117(1–2),** 43 (1995).

13. S.H. Yun, G.J. Tearney, B.E. Bouma, B.H. Park and J.F. de Boer, "High-speed optical frequency-domain imaging at 1.3 μm", *Opt. Express* **11(26),** 3598 (2003). doi: 10.1364/OE.11.003598

14. B.E. Bouma, S.H. Yun, B.J. Vakoc, M.J. Suter and G.J. Tearney, "Fourier-domain optical coherence tomography: Recent advances toward clinical utility", *Curr. Opin. Biotechnol.* **20,** 111 (2009). doi: 10.1016/j.copbio.2009.02.007

15. B. Liu and M.E. Brezinski, "Theoretical and practical considerations on detection performance of time domain, Fourier domain and swept source optical coherence tomography", *J. Biomed. Opt.* **12(4),** 044007 (2007). doi: 10.1117/1.2753410

16. R. LeiTgeb, C.K. Hitzenberger and A.F. Fercher, "Performance of Fourier domain vs. time domain optical coherence tomography", *Opt. Express* **11(8),** 889 (2003). doi: 10.1364/OE.11.000889

17. S.H. Yun, G.J. Tearney, J.F. de Boer and B.E. Bouma, "Motion artifacts in optical coherence tomography with frequency-domain ranging", *Opt. Express* **12(13),** 2977 (2004). doi: 10.1364/OPEX.12.002977

18. M. Wojtkowski, "High-speed optical coherence tomography: Basics and applications", *Appl. Opt.* **49(16),** D30 (2010). doi: 10.1364/AO.49.000D30

19. M.D. Kulkarni and J.A. Izatt, "Spectroscopic optical coherence tomography", Conference on Lasers and Electro-Optics 1996, OSA Technical Digest Series. Optical Society of America, Washington, DC, USA, p. 59 (1996).

20. U. Morgner, W. Drexler, F.X. Kartner, X.D. Li, C. Pitris, E.P. Ippen and J.G. Fujimoto, "Spectroscopic optical coherence tomography", *Opt. Lett.* **25(2),** 111 (2000). doi: 10.1364/OL.25.000111

21. C. Xu, F. Kamalabadi and S.A. Boppart, "Comparative performance analysis of time–frequency distributions for spectroscopic optical coherence tomography", *Appl. Opt.* **44(10),** 1813 (2005). doi: 10.1364/AO.44.001813

22. R. Leitgeb, M. Wojtkowski, A. Kowalczyk, C.K. Hitzenberger, M. Sticker and A.F. Fercher, "Spectral measurement of absorption by spectroscopic frequency-domain optical coherence tomography.", *Opt. Lett.* **25(11),** 820 (2000). doi: 10.1364/OL.25.000820

23. A.L. Oldenburg, C. Xu and S.A. Boppart, "Spectroscopic optical coherence tomography and microscopy", *IEEE J. Sel. Top. Quantum Electron.* **13(6),** 1629 (2007). doi: 10.1109/JSTQE.2007.910292

24. B. Hermann, B. Hofer, C. Meier and W. Drexler, "Spectroscopic measurements with dispersion encoded full range frequency domain optical coherence tomography in single- and multilayered non-scattering phantoms", *Opt. Express* **17(26),** 24162 (2009). doi: 10.1364/OE.17.024162

25. P. Steiner, C. Meier and V.M. Koch, "Influence and compensation of autocorrelation terms in depth-resolved spectroscopic Fourier-domain optical coherence tomography", *Appl. Opt.* **49(36),** 6917 (2010). doi: 10.1364/AO.49.006917

26. C. Xu, P.S. Carney and S.A. Boppart, "Wavelength-dependent scattering in spectroscopic optical coherence tomography", *Opt. Express* **13(14),** 5450 (2005). doi: 10.1364/OPEX.13.005450

27. C. Xu, J. Ye and D.L. Marks, "Near-infrared dyes as contrast-enhancing agents for spectroscopic optical coherence tomography", *Opt. Lett.* **29(14),** 1647 (2004). doi: 10.1364/OL.29.001647

28. H. Cang, T. Sun, Z.Y. Li, J. Chen, B.J. Wiley, Y. Xia and X. Li, "Gold nanocages as contrast agents for spectroscopic optical coherence tomography", *Opt. Lett.* **30(22),** 3048 (2005). doi: 10.1364/OL.30.003048

29. R.N. Graf, F.E. Robles, X. Chen and A. Wax, "Detecting precancerous lesions in the hamster cheek pouch using spectroscopic white-light optical coherence tomography to assess nuclear morphology via spectral oscillations", *J. Biomed. Opt.* **14(6),** (2009). doi: 10.1117/1.3269680

30. P. Carmeliet and R.K. Jain, "Angiogenesis in cancer and other disease", *Nature* **407(6801),** 249 (2000). doi: 10.1038/35025220

31. D.J. Faber, E.G. Mik, M.C.G. Aalders and T.G. van Leeuwen, "Light absorption of (oxy-)hemoglobin assessed by spectroscopic optical coherence tomography", *Opt. Lett.* **28(16),** 1436 (2003). doi: 10.1364/OL.28.001436

32. D.J. Faber, E.G. Mik, M.C.G. Aalders and T.G.V. Leeuwen, "Toward assessment of blood oxygen saturation by spectroscopic optical coherence tomography", *Opt. Lett.* **30(9),** 1015 (2005). doi: 10.1364/OL.30.001015

33. C.W. Lu, C.K. Lee, M.T. Tsai, Y.M. Wang and C.C. Yang, "Measurement of the hemoglobin oxygen saturation level with spectroscopic spectral-domain optical coherence tomography", *Opt. Lett.* **33(5),** 416 (2008). doi: 10.1364/OL.33.000416

34. J. Yi and X. Li, "Estimation of oxygen saturation from erythrocytes by high-resolution spectroscopic optical coherence tomography", *Opt. Lett.* **35(12),** 2094 (2010). 10.1364/OL.35.002094

35. X. Liu and J.U. Kang, "Depth-resolved blood oxygen saturation assessment using spectroscopic common-path

Fourier domain optical coherence tomography", *IEEE Transact. Biomed. Eng.* **57(10),** 2572 (2010). doi: 10.1109/TBME.2010.2058109

36. F.E. Robles, S. Chowdhury and A. Wax, "Assessing hemoglobin concentration using spectroscopic optical coherence tomography for feasibility of tissue diagnostics", *Biomed. Opt. Express* **1(1),** 310 (2010). doi: 10.1364/BOE.1.000310

37. P. Cimalla, J. Walther, M. Mehner, M. Cuevas and E. Koch, "Simultaneous dual-band optical coherence tomography in the spectral domain for high resolution *in vivo* imaging", *Opt. Express* **17(22),** 19486 (2009). doi: 10.1364/OE.17.019486

38. F. Spöler, S. Kray, P. Grychtol, B. Hermes, J. Bornemann, M. Först and H. Kurz, "Simultaneous dual-band ultra-high resolution optical coherence tomography", *Opt. Express* **15(17),** 10832 (2007). doi: 10.1364/OE.15.010832

39. D. Sacchet, J. Moreau, P. Georges and A. Dubois, "Simultaneous dual-band ultra-high resolution full-field optical coherence tomography", *Opt. Express* **16(24),** 19434 (2008). doi: 10.1364/OE.16.019434

40. L. Vabre, A. Dubois and A.C. Boccara, "Thermal-light full-field optical coherence tomography", *Opt. Lett.* **27(7),** 530 (2002). doi: 10.1364/OL.27.000530

41. A. Dubois, K. Grieve, G. Moneron, R. Lecaque, L. Vabre and C. Boccara, "Ultrahigh-resolution full-field optical coherence tomography", *Appl. Opt.* **43(14),** 2874 (2004). doi: 10.1364/AO.43.002874

42. S. Kray, F. Spöler, M. Först and H. Kurz, "High-resolution simultaneous dual-band spectral domain optical coherence tomography", *Opt. Lett.* **34(13),** 1970 (2009). doi: 10.1364/OL.34.001970

43. P. Matousek and N. Stone, "Emerging concepts in deep Raman spectroscopy of biological tissue", *Analyst* **134,** 1058 (2009). doi: 10.1039/b821100k

44. C.A. Patil, J. Kalkman, D.J. Faber, J.S. Nyman, T.G. van Leeuwen and A. Mahadevan-Jansen, "Integrated system for combined Raman spectroscopy–spectral domain optical coherence tomography", *J. Biomed. Opt.* **16(1),** 011007 (2011). doi: 10.1117/1.3520132

45. C.A. Patil, H. Kirshnamoorthi, D.L. Ellis, T.G. van Leeuwen and A. Mahadevan-Jansen, "A clinical instrument for combined Raman spectroscopy–optical coherence tomography of skin cancers", *Lasers Surg. Med.* **43,** 143 (2011). doi: 10.1002/lsm.21041

46. A.C.T. Ko, L.P. Choo-Smith, M. Hewko, L. Leonardi, M.G. Sowa, C.C.S. Dong, P. Williams and B. Cleghorn, "*Ex vivo* detection and characterization of early dental caries by optical coherence tomography and Raman spectroscopy", *J. Biomed. Opt.* **10(3),** 031118 (2005). doi: 10.1117/1.1915488

47. J.W. Evans, R.J. Zawadzki, R. Liu, J.W. Chan, S.M. Lane and J.S. Werner, "Optical coherence tomography and Raman spectroscopy of the *ex-vivo* retina", *J. Biophoton.* **2(6–7),** 398 (2009). doi: 10.1002/jbio.200910022

48. C.A. Patil, N. Bosschaart, M.D. Keller, T.G. van Leeuwen and A. Mahadevan-Jansen, "Combined Raman spectroscopy and optical coherence tomography device for tissue characterization", *Opt. Lett.* **33(10),** 1135 (2008). doi: 10.1364/OL.33.001135

49. K. Doi, "Computer-aided diagnosis in medical imaging: Historical review, current status and future potential", *Comput. Med. Imaging Graphics* **31,** 198 (2007). doi: 10.1016/j.compmedimag.2007.02.002

50. J. Rogowska, "Digital image processing techniques for speckle reduction, enhancement and segmentation of optiical coherence tomography (OCT) images", in *Optical Coherence Tomography: Principles and Application*, Ed by M. Brezinski. Academic Press, Boston, USA (2006).

51. R.C. Gonzalez and R.E. Woods, *Digital Image Processing*, 3rd Edn. Pearson Prentice Hall, New Jersey, USA (2008).

52. K. Kallenbach and J. Frederiksen, "Optical coherence tomography in optic neuritis and multiple sclerosis: a review", *Eur. J. Neurol.* **14,** 841 (2007). doi: 10.1111/j.1468-1331.2007.01736.x

53. A.P.D. Henderson, D.R. Altmann, A.S. Trip, C. Kallis, S.J. Jones, P.G. Schlottmann, D.F. Garway-Heath, G.T. Plant and D.H. Miller, "A serial study of retinal changes following optic neuritis with sample size estimates for acute neuroprotection trials", *Brain* **133,** 2592 (2010). doi: 10.1093/brain/awq146

54. A.M. Bagci, M. Shahidi, R. Ansari, M. Blair, N.P. Blair and R. Zelkha, "Thickness profiles of retinal layers by optical coherence tomography image segmentation", *Am. J. Ophthalmol.* **146,** 679 (2008). doi: 10.1016/j.ajo.2008.06.010

55. M.K. Garvin, M.D. Abràmoff, R. Kardon, S.R. Russell, X. Wu and M. Sonka, "Intraretinal layer segmentation of macular optical coherence tomography images using optimal 3-D graph search", *IEEE Trans. Med. Imaging* **127(10),** 1495 (2008). doi: 10.1109/TMI.2008.923966

56. M.K. Garvin, M.D. Abràmoff, X. Wu, S.R. Russell, T.L. Burns and M. Sonka, "Automated 3-D intraretinal layer segmentation of macular spectral-domain optical coherence tomography images", *IEEE Trans. Med. Imaging* **28(9),** 1436 (2009). doi: 10.1109/TMI.2009.2016958

57. V. Kajic, B. Považay, B. Hermann, B. Hofer, D. Marshall, P.L. Rosin and W. Drexler, "Robust segmentation of intra-retinal layers in the normal human fovea using a novel statistical model based on texture and shape analysis", *Opt. Express* **18(14),** 14730 (2010).

58. S. Lu, C.Y.I. Cheung, J. Liu, J.H. Lim, C.K.S. Leung and T.Y. Wong, "Automated layer segmentation of optical coherence tomography images", *IEEE Trans. Biomed. Eng.* **57(10),** 2605 (2010). doi: 10.1109/TBME.2010.2055057

59. J. Canny, "A computational approach to edge detection", *IEEE Trans. Pattern Anal. Machine Intell.* **8(6),** 679 (1986). doi: 10.1109/TPAMI.1986.4767851